Reprinted from the JOURNAL OF LUBRICATION TECHNOLOGY, *Vol. 99, No. 2, April 1977*

Systems of Finite Elements for Finite Bearings

P. E. Allaire
Assistant Professor.

J. C. Nicholas
Research Associate.

E. J. Gunter
Professor.

Department of Mechanical Engineering, University of Virginia, Charlottesville, Va.

Systems of finite elements are organized using matrix notation for finite length bearings. Most fluid film bearings have surface areas which can be divided into a grid of elements whose nodes are labeled in matrix form. The resulting equations for nodal pressures are block tridiagonal and the solution is easily obtained with direct methods. Analysis of both general slider and journal bearings is included. The choice of how the film is divided into elements can significantly affect the error involved in the numerical solution and some criteria are developed for optimizing the division scheme. In the analysis of a square squeeze pad of uniform thickness, choosing the diagonal sides of elements nearly perpendicular to the pressure gradient direction gives an error in the calculated load carrying capacity of over two times that obtained by aligning element diagonal sides approximately with the pressure gradient direction. For rotating bearings, varying the grid spacing in the circumferential direction directly as the film thickness and properly choosing diagonal alignment can significantly reduce computer time.

1 Introduction

Major advantages of the finite element approach accrue from its total generality with regard to geometry and boundary conditions. Elements can approximate any boundary shape such as curved hydrostatic bearings or oil inlet geometry. Use of elements and interpolation functions which insure continuity of pressure and mass rate of flow across interelement boundaries permit the analysis of films with steps such as those found in pressure dam or spiral groove bearings. Either pressure or oil flow type boundary conditions are easily included. Finally, the bearing surface can be divided up various ways and the particular scheme should be chosen to minimize the error in the numerical method.

The finite element method has been used in the solution of fluid film lubrication problems for some years. Since Zienkiewicz and Cheng [1, 2][1] first recognized that finite elements could be applied to field problems, other works have expanded and developed the method. Reddi, et al. [3, 4] noted that the system of algebraic equations generated for the nodal pressures is a banded, symmetric matrix which may be solved directly with minimal requirements of computer storage and time. As noted by Hays [5], it is desirable to number the nodes to minimize the matrix bandwidth. Wada, et al. [6, 7] showed that finite elements may produce more accurate solutions for journal bearings than finite differences. The disadvantages of the rectangular element developed for finite bearings [7] are that continuity is not satisfied along the interelement boundaries and that the only bearing geometry easily analyzed is a rectangular one. Allan [8] has applied the method to hydrodynamic and externally pressurized pocket bearings using a simple iterative scheme to evaluate the nodal pressures.

More recent works have dealt with generalizations of the method. An introduction to both the direct method for infinitely long bearings and a variational approach is given by Booker and Huebner [9]. Oden [10] has developed general nomenclature techniques for other problems which are utilized here. Finite elements have also been employed in the solution of EHD and transient problems [11]. Oh and Huebner [12] have solved a complete elastohydrodynamic finite journal bearing problem. The problem of thermal effects in lubrication has been considered by both Tieu [13] and Huebner [14]. Shelly and Ettles [15] have developed a one-dimensional approximation for bearings using exponential elements. The most recent and extensive treatment of fluid film lubrication is in a textbook which devotes an entire chapter to the subject [16].

The present study develops a systematic matrix approach for finite elements directly from a variational principle for the pressure. The fluid pressure, velocity, density, and viscosity are assumed constant across the film, but may vary over the length of the bearing. Also the film thickness, velocities of the upper and lower surfaces, and squeeze velocities may vary over the length of the bearing. Thus, within certain limits, this analysis applies to compressible, variable viscosity flows (using an iterative process since ρ and μ are functions of p).

One purpose of the present work is to develop a systematic matrix approach for finite elements which automatically produces a minimum bandwidth of algebraic equations Most finite fluid film bearings such as plain journal, pressure dam, squeeze pad, and tilting pad have

[1] Numbers in brackets designate References at end of paper.

Contributed by the Lubrication Division and presented at the Joint Lubrication Conference, Boston, Mass., October 5–7, 1976, of THE AMERICAN SOCIETY OF MECHANICAL ENGINEERS. Manuscript received by the Lubrication Division April 2, 1975; revised manuscript received June 2, 1976. Paper No. 76-Lub-13.

surface areas which can be divided into a grid whose nodes are labeled in matrix form. Note that the grid is *not* required to be rectangular in form, but that the nodal coordinates and nodal pressures can be organized into M rows and N columns of an $M \times N$ array or matrix. This allows the concentration of nodes near oil supply holes, pressure dams, or simply in regions where large variations in pressure occur (as is currently done for finite elements in stress analysis near a hole). By organizing the labeling in matrix form throughout the analysis, the solution is easily obtained with the direct Gaussian elimination method for block tridiagonal matrices [17] or other methods.

The other purpose of this study is to obtain insight into the optimum methods for dividing the bearing area into elements. An analysis of the error produced in solving the uniform rectangular squeeze pad and journal bearing using various uniform and variable grid spacings shows that the best choice of division scheme can substantially reduce the number of nodes required and thus the computer costs. Thus far this type of study has not been carried out for lubrication problems.

Only triangular elements and linear interpolation functions for the pressure within them are used. Analysis of more complex finite elements has usually shown little advantage over simply increasing the number of elements if increased accuracy is desired [18].

2 Finite Element Formulation

Consider a general finite slider bearing of area A such as shown in Fig. 1. The pressure must minimize the functional [9]

$$J(P) = \iint_A \left\{ \frac{\rho h^3}{24\mu}\left[\left(\frac{\partial P}{\partial x}\right)^2 + \left(\frac{\partial P}{\partial y}\right)^2\right] - \rho h\left[U_x \frac{\partial P}{\partial x} + U_y \frac{\partial P}{\partial y}\right] + \frac{\partial}{\partial t}(\rho h)P \right\} dA + \int_{C_q} [q_x n_x + q_y n_y)P]\, dC \quad (1)$$

with the boundary conditions such that along part of the boundary, C_p, the pressure is specified

$$[P]_{\text{on } C_p} = [P_a]_{\text{on } C_p} \quad (2)$$

and along the remainder of the boundary, C_q, the mass rate of flow is specified

$$[q_x]_{\text{on } C_q} = [q_{ax}]_{\text{on } C_q} \quad (3a)$$

$$[q_y]_{\text{on } C_q} = [q_{ay}]_{\text{on } C_q} \quad (3b)$$

The values of P_a and q_a may vary around the boundary. If the pressure is specified around the entire boundary, $C_p = C$, the last integral in equation (1) is simply ignored.

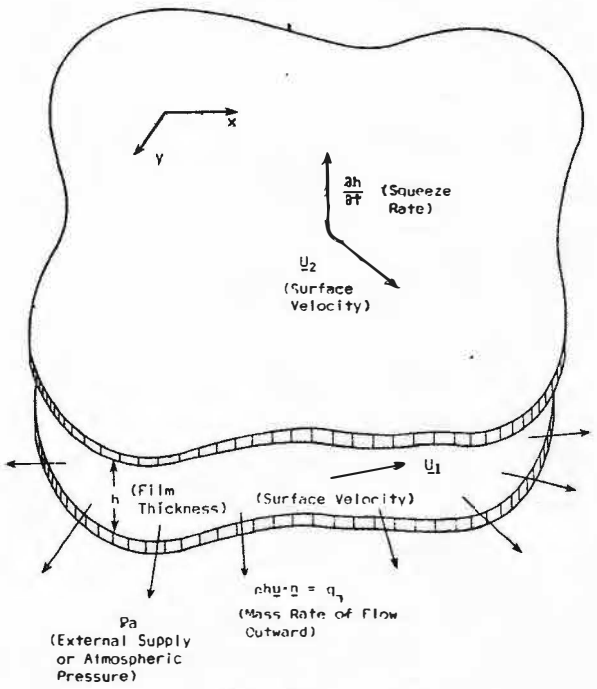

Fig. 1 Fluid film geometry

The fluid film must be divided into a global system of elements in a manner such as that shown in Fig. 2. First the bearing surface is divided into $M - 1$ quadrilaterals in the y direction and $N - 1$ quadrilaterals in the x direction as in Fig. 2(a). This permits the nodes at the intersections to be labeled in a rectangular matrix of order $M \times N$. Two subscripts are required to identify a particular node. Second, the quadrilaterals are divided into triangular elements of type 1–2 or type 3–4 as shown in Fig. 2(b). Now three superscripts are used to identify the element properties. The first two superscripts indicate the upper left node and the third gives the type of element. For this system the number of elements E is given by $2(M - 1)(N - 1)$.

The local labeling system used within the eth node starts with labeling the node opposite the diagonal with i and continuing with j, k in the clockwise direction as shown in Fig. 3. Each of the nodal pressures P_i, P_j, P_k are labeled correspondingly and the coordinates of the nodes are denoted by (x_i, y_i), (x_j, y_j), (x_k, y_k). These local properties within an element have a single subscript while the global system considering all of the elements has two subscripts corresponding to a matrix notation.

Nomenclature

A = area of bearing, element
b_n, c_n = element constants, $n = i, j, k$
C = boundary of finite bearing
C_p, C_q = boundary on which pressure, mass flow are specified
e = element
E = total number of elements
h = film thickness
$\dot{h}$ = squeeze velocity
i, j, k = nodes of triangular element labeled in clockwise order, local labeling
I, J = nodes of bearing in y and x directions, global labeling
$J(P)$ = functional
K_h = squeeze fluidity component
K_p = pressure fluidity component
K_{Ux}, K_{Uy} = shear fluidity components in x, y directions
m, n = nodal indices, i, j, k for finite bearings
M, N = number of nodes in approximate y, x directions
n_x, n_y = unit vectors in x, y directions
P, P_a = pressure, pressure specified on C_p
q, q_x, q_y, q_a = mass rate of flow, in x and y directions, mass rate of flow specified on C_q
r = ratio of successive grid spacings
R = radius of shaft (journal)
t = time
$\mathbf{U}$ = Average surface velocity, vector, $\mathbf{U} = 1/2(\mathbf{U}_1 + \mathbf{U}_2)$
$\mathbf{U}_1$ = velocity of lower surface of slider, vector
$\mathbf{U}_2$ = velocity of upper surface of slider, vector
U_x, U_y = vector component of $\mathbf{U}$ in x, y directions
W = weight
x, y = Cartesian coordinates
$\Delta x, \Delta y$ = grid spacing in x, y directions
z = axial coordinate
ϵ = error
θ = circumferential coordinate around circular bearing
ρ = fluid density
μ = fluid viscosity
ω_j, ω_b = angular velocity of journal, bushing in counterclockwise

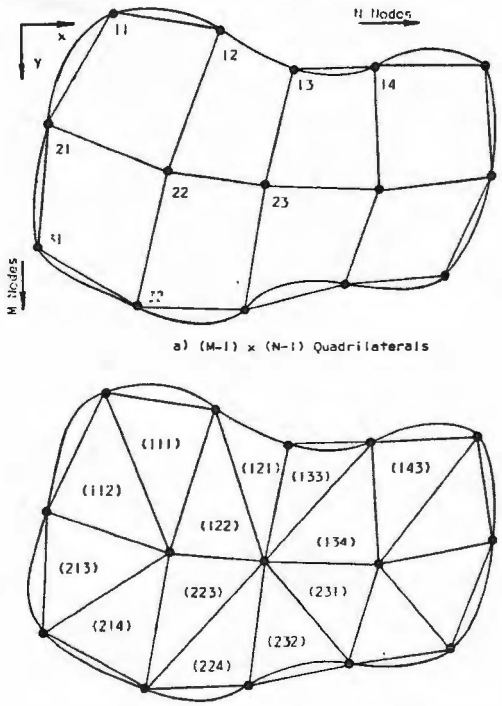

Fig. 2 Dividing fluid film into elements

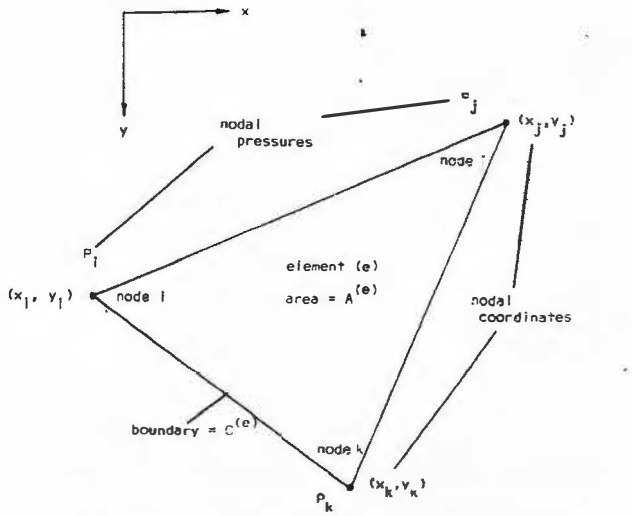

Fig. 3 The *e*th triangular element with a node located at each corner. Nodes are labeled clockwise.

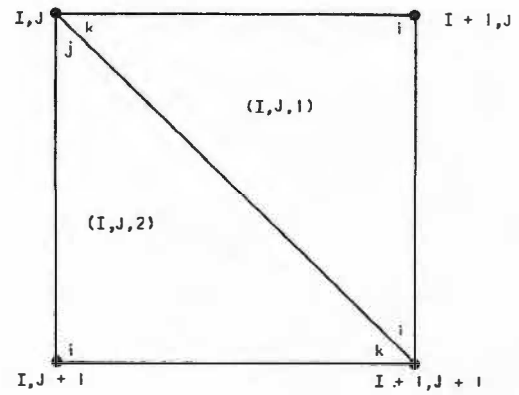

Fig. 4 Local and global labeling systems for the elements associate with the *I*, *J*th node

Fig. 4 shows the four different types of elements with both local and global labeling systems. All four elements are related to the I, Jth element in the upper left-hand corner, and the local labeling system is related to the global system as shown in Table 1. Two labeling systems, local and global, avoid the use of four subscripts or superscripts in describing a node.

The complete finite element formulation for the general slider and rotating bearing is given in the Appendix. The matrix equations are in the block tridiagonal form suitable for direct solution using banded Gauss elimination [17]. The solution technique involves the inversion of N square matrices of order $M \times M$ so that M should always be chosen as the smaller number of M and N.

3 Rectangular Squeeze Pad Analysis

A square squeeze pad with uniform film thickness is employed [9] as an example. The sides are of length unity and the other properties are given by

ρ	$= 12$	(density)
μ	$= 2 \times 10^{-6}$	(viscosity)
h	$= 1 \times 10^{-2}$	(film thickness)
$\partial h/\partial t$	$= -1$	(squeeze velocity)

Because of symmetry about the x and y axes, analysis of only one quadrant is necessary. An analysis using nine equally spaced nodes and eight 1–2 type elements were carried out with the solution

$$[P] = \begin{bmatrix} 1.8750 & 1.3750 & 0 \\ 1.3750 & 1.0625 & 0 \\ 0 & 0 & 0 \end{bmatrix}$$

Integrating the pressure over all of the elements, the weight carried by the pad is calculated as $W = 0.766$.

Carrying out a similar analysis using finite differences for purposes of comparison gives the solution

$$[P] = \begin{bmatrix} 1.687 & 1.312 & 0 \\ 1.312 & 1.030 & 0 \\ 0 & 0 & 0 \end{bmatrix}$$

Calculating the load carrying capacity by the same method as for the finite element solution gives $W = 0.726$.

Table 1 Local and global labeling systems

Global labeling system	Local labeling system			
Element				
e	i	j	k
$(I, J, 1)$	$(I+1, J)$	$(I+1, J+1)$	(I, J)
$(I, J, 2)$	$(I, J+1)$	(I, J)	$(I+1, J+1)$
$(I, J, 3)$	(I, J)	$(I+1, J)$	$(I, J+1)$
$(I, J, 4)$	$(I+1, J+1)$	$(I, J+1)$	$(I+1, J)$

The exact solution obtained from Hays [19] is evaluated at the nodal points to give

$$[P] = \begin{bmatrix} 1.769 & 1.377 & 0 \\ 1.377 & 1.087 & 0 \\ 0 & 0 & 0 \end{bmatrix}$$

and the load carrying capacity $W = 0.849$. The finite element errors in the nodal pressures are

$$[\epsilon]_{FEM} = \begin{bmatrix} 6.0\% & -0.1\% & 0 \\ -0.1\% & -2.2\% & 0 \\ 0 & 0 & 0 \end{bmatrix}$$

and for the finite differences they are

$$[\epsilon]_{FDM} = \begin{bmatrix} -4.6\% & -4.7\% & 0 \\ -4.7\% & -5.1\% & 0 \\ 0 & 0 & 0 \end{bmatrix}$$

These comparisons show that the finite element solution is sometimes above and sometimes below the exact solution while the finite difference solution is consistently below the actual value. Thus the weight carried as evaluated with finite elements is in error by 9.8 percent and with finite differences is 15.0 percent in error.

If only two type 1–2 elements with four nodes are used, the finite element solution for the only unknown node is $P_{11} = 2.0$ and $W = 0.67$ while the finite difference method with only one node gives $P_{11} = 1.50$ and $W = 0.50$ compared to the exact solution $P_{11} = 1.77$. Using two type 3–4 elements so that the diagonal goes from lower left to upper right gives $P_{11} = 2.0$ and $W = 0.33$. The error in W with 1–2 finite elements and finite differences are 21 and 41 percent, respectively. With the 3–4 elements the value of P_{11} is the same as for the 1–2 elements, but the error in W is 61 percent because the type 4 element has zero pressure (all three nodes are zero) so it carries no load.

Another study of various methods of dividing up the lower one-half of the squeeze pad into elements is shown in Fig. 5 and Table 2. The most effective method of choosing elements is choosing diagonals (FEM #1) so that they are aligned with the pressure gradient direction which is radially outward from the origin of the xy coordinate system. The worst choice is diagonals nearly perpendicular to the pressure gradient direction (FEM #3). Table 2 shows that the error for FEM #3 is 2.3 times the error for FEM #1 when 45 nodes are used. One reason is that the pressure over the entire element on each outside corner is zero since the three corresponding nodal pressures are all zero. Thus the corner elements make no contribution to the load carrying capacity if FEM #3 is used. Method FEM #2 has been used by other authors [9], but it gives significantly larger errors.

Another study was carried out to evaluate the effect of varying the grid spacing to concentrate the elements either in the center or near the edge of the pad. The quarter pad was divided into squares whose successive side lengths increased or decreased by the ratio r in a geometric series. The optimum finite element method (FEM #1) was used for all values of r. For this example the lowest error occurred with $r = \frac{1}{2}$ when a small number of elements was used and $r = \frac{3}{4}$ when the number of elements was increased (Table 3). Thus concentrating the nodes more toward the outer edge increased the accuracy, but not by more than a small percentage.

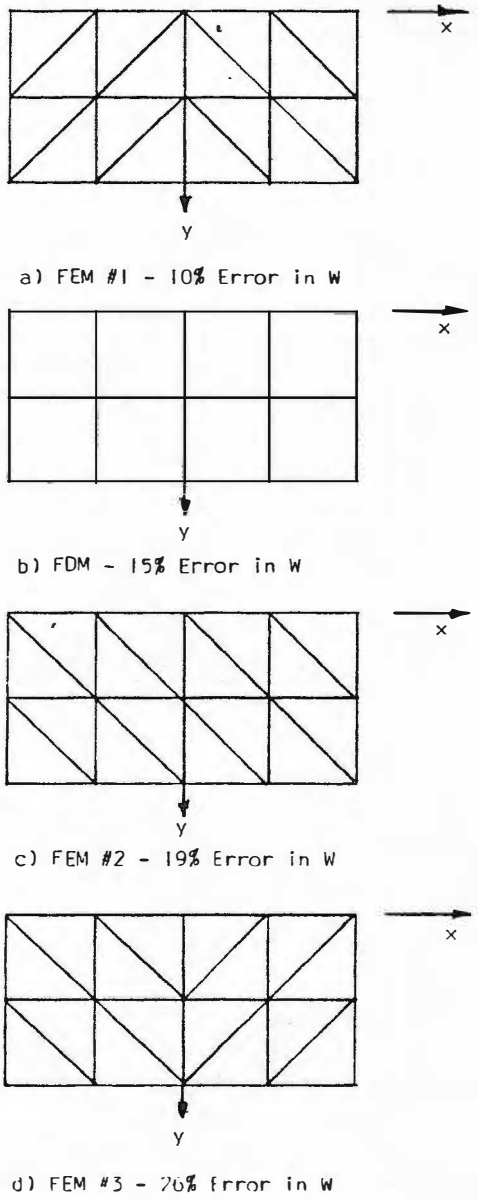

Fig. 5 Comparison of error for square squeeze pad using the lower half of a square squeeze pad

Table 2 Comparison of error in finite element and finite difference numerical solutions for one-half of square squeeze pad

Number of nodes used in half pad	% Error in weight capacity			
	FEM #1	FDM	FEM #2	FEM #3
15 (3 x 5)	9.8	15.0	18.6	26.4
28 (4 x 7)	5.2	7.2	9.1	12.8
45 (5 x 9)	3.4	4.5	5.5	7.7

4 Journal Bearing Analysis

The effects of variable grid spacing and diagonal alignment were further investigated for the more practical problem of a plain journal

Table 3 Comparison of errors in finite differences and finite elements using variable grid spacing for square squeeze pad. The parameter r is the ratio of successive grid spacings

Total number of nodes in quadrant	Percentage error in weight carried by squeeze pad: Finite differences	Finite elements using variable grid spacing: $r = \frac{1}{2}$	$r = \frac{3}{4}$	$r = 1$	$r = \frac{3}{2}$
4 (2 × 2)	41%	21%	21%	21%	21%
9 (3 × 3)	15%	7.6%	8.3%	9.8%	13%
16 (4 × 4)	7.2%	4.5%	4.1%	5.2%	8.8%
25 (5 × 5)	4.5%	3.6%	2.6%	3.4%	7.1%

Table 4 Comparison of the errors of the finite element method for a plain journal bearing considering variable and equal grids and two types of diagonal alignment

Number of nodes ($M \times N$)	Variable grids FEM #1 (% Error)	Equal grids FEM #1 (% Error)	Variable grids FEM #2 (% Error)	Equal grids FEM #2 (% Error)
5 × 41	2.7	3.3	3.6	3.9
4 × 41	4.4	5.1	5.6	5.8
3 × 41	9.2	10.1	10.9	11.0
5 × 31	3.3	4.2	4.4	4.9
4 × 31	4.9	6.0	6.4	6.8
3 × 31	9.5	10.7	11.8	12.1
5 × 21	4.7	6.8	6.5	7.6
4 × 21	6.3	8.4	8.6	9.6
3 × 21	10.7	13.0	14.1	14.8
5 × 11	12.5	19.8	15.5	20.6
4 × 11	13.6	21.2	17.7	22.2
3 × 11	17.1	25.0	23.2	26.6

bearing. It was assumed that the lubricant was incompressible and isoviscous with the properties

R = 1.27 cm (0.5 in.)
L = 2.54 cm (1.0 in.)
c = 0.0127 cm (0.005 in.)
ω_j = 314.2 rad/s (3,000 rev/min)
μ = 1.24×10^{-6} N-s/cm^2 (1.8×10^{-6} reyns)

Due to symmetry only one-half of the bearing was analyzed. The bearing surface was divided into M nodes in the axial direction for one-half of the bearing length and N nodes in the circumferential direction.

Finite element solutions for several cases were obtained using the formulation presented in the Appendix. The load capacity was calculated after neglecting negative pressures to account for cavitation. The bearing eccentricity was taken as 0.5657 and the attitude angle as 45 deg. The finite element results are compared to an analytical solution to the problem [19] which gave a load capacity of 25.429 N (5.717 lb) when negative pressures are neglected.

The results for four cases are shown in Table 4. In the first method, the grid spacing was varied in direct proportion to the film thickness while the diagonals were aligned as in FEM #1 for the half squeeze pad. The second method was the same except that the grid spacing was constant. For comparison, methods 3 and 4 represent aligning all of the diagonals in the same direction as used in FEM #2 for the half squeeze pad with both variable and equal grid spacing, respectively. In all cases the axial grid spacing was taken as equal.

As shown in Table 4, concentrating grid points where the pressure gradient is a maximum (near the minimum film thickness) and aligning the diagonals to best approximate the direction of the pressure gradient over most of the bearing produces the least percent of error for a given number of nodes. The error given by methods 2 and 3 shows that the effect of variable grid spacing and diagonal alignment is cumulative in improvement over method 4. In nearly all cases the error using method 1 was approximately two-thirds of method 4.

Consider the case of 4 × 31 nodes using method 1 and 5 × 31 nodes using method 4 since both gave 4.9 percent error. If a banded Gaussian elimination scheme is used, it requires the inversion of N square matrices of order M by M. Inversion of a square matrix requires approximately $M^3/3$ operations so that the use of method 1 results in a nearly 50 percent saving in computer time for this portion of the analysis. As the number of circumferential grid points is reduced to 11, this effect becomes more pronounced. A 3 × 11 grid using method 1 is more accurate than a 5 × 11 grid using method 4 while the number of operations is over four times as large.

5 Discussion of Results and Conclusions

The finite element method has been fully developed in matrix form for those lubrication problems which can be divided up into elements suitable for labeling in an M by N matrix. Complete flexibility with regard to bearing geometry and boundary conditions has been retained. The resulting matrix equations for the nodal pressures are block tridiagonal in form. The bandwidth is minimized due to the formulation of the problem permitting a noniterative solution reducing computer storage and time.

Analysis of the square squeeze pad showed that different types of boundary conditions, pressure, and mass rate of flow are automatically included in the finite element formulation of the problem. The finite difference formulation is simpler but must be modified to include four artificial nodes. The error analysis carried out indicates that the division of the bearing surface into elements is of importance if the lowest computation time is desired for a given level of accuracy. For the squeeze pad obtaining approximately 4 percent accuracy would require only 16 nodes if the best division scheme (FEM #1, $r = \frac{3}{4}$) were used, but 36 nodes if a poor division scheme (FEM #3, uniform spacing) were used. Clearly, a finite element computer program should be set up to automatically divide the fluid film into elements to minimize the error. Usually some clues as to the direction of the pressure gradient in the bearing are available before the problem is solved. These clues can be used by the programmer to align the diagonal sides of elements in the expected direction of the pressure gradient where possible.

The journal bearing analysis revealed that both diagonal alignment and grid spacing are important in reducing error for a given number of nodes. When the grid spacing was varied directly as the film thickness and the diagonal sides of elements were aligned approxi-

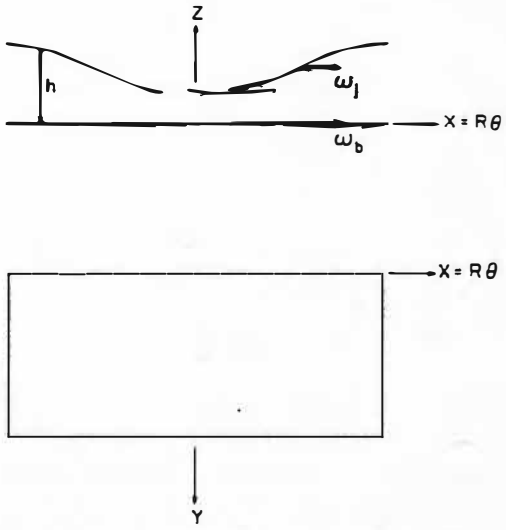

Fig. 6 Journal bearing split at maximum film thickness

mately with the pressure gradient direction, a significant reduction in the number of operations required to invert the block tridiagonal matrices resulted. This reduction is of particular importance in reducing computer time for a variety of practical problems. For example, a nonlinear time-transient analysis requires the calculation of the nodal pressures for each time step. Another example would be a finite element tilting pad bearing program that calculates equilibrium position and bearing characteristics. The nodal pressure field must be determined for each pad iteration. A similar example is a finite element gas bearing program where an iterative procedure is required since the density variation is a function of the pressure field. Because of the iterative procedures involved in each case mentioned before, the number of times the nodal pressures are calculated is increased manyfold magnifying the importance of proper grid spacing and diagonal alignment in keeping computer time to a minimum.

The journal bearing analysis also showed that as the grid becomes coarser (number of nodes reduced) it becomes more desirable to use variable grid spacing and proper diagonal alignment. Often a coarse grid is required because of limitations on computer time. For example, consider a bearing program that determines equilibrium position and bearing characteristics. A coarse grid may be used first to determine an approximate equilibrium position. Then, the number of nodes may be increased and a more exact equilibrium position determined.

References

1 Zienkiewicz, O. C., and Cheng, Y. K., *The Finite Element Method in Structural and Continuum Mechanics*, McGraw-Hill, London, 1967.

2 Zienkiewicz, O. C., and Cheng, Y. K., "Finite Elements in the Solution of Field Problems," *The Engineer*, Vol. 24, 1968, pp. 507–510.

3 Reddi, M. M., "Finite-Element Solution of the Incompressible Lubrication Problem," JOURNAL OF LUBRICATION TECHNOLOGY, TRANS. ASME, Series F, Vol. 91, No. 3, July 1969, pp. 524–533.

4 Reddi, M. M., and Chu, T. Y., "Finite-Element Solution of the Steady-State Compressible Lubrication Problem," JOURNAL OF LUBRICATION TECHNOLOGY, TRANS. ASME, Series F, Vol. 22, No. 3, July 1970, pp. 495–503.

5 Hays, D. F., Discussion of Reference [4].

6 Wada, S., Hayaski, H., and Migita, M., "Application of Finite Element Method to Hydrodynamic Lubrication Problems (Part I, Infinite-Width Bearings)," *Bulletin of Japan Society of Mechanical Engineers*, Vol. 14, No. 77, Nov. 1971, pp. 1222–1233.

7 Wada, S., and Hayaski, H., "Application of the Finite Element Method to Hydrodynamic Lubrication Problems (Part 2, Finite Width Bearings)," *Bulletin of Japan Society of Mechanical Engineers*, Vol. 14, No. 77, Nov. 1971, pp. 1234–1244.

8 Allan, T., "The Application of Finite Element Analysis of Hydrodynamic and Externally Pressurized Pocket Bearings," *Wear*, Vol. 19, Feb. 1972, pp. 169–206.

9 Booker, J. F., and Huebner, K. H., "Application of Finite Elements to Lubrication: An Engineering Approach," JOURNAL OF LUBRICATION TECHNOLOGY, TRANS. ASME, Series F, Vol. 24, No. 4, Oct. 1972, pp. 313–323.

10 Oden, J. T., *Finite Elements of Nonlinear Continua*, McGraw-Hill, New York, 1972.

11 Zienkiewicz, O. C., and Taylor, C., "Weighted Residual Processes in Finite Element with Particular Reference to Some Transient and Coupled Problems," in *Lectures on Finite Element Methods in Continuum Mechanics*, Oden, J. T., ed., University of Alabama Press, Huntsville. 1973.

12 Oh, K. P., and Huebner, K. H., "Solution of Elastohydrodynamic Finite Journal Bearing Problem," JOURNAL OF LUBRICATION TECHNOLOGY, TRANS. ASME, Series F, Vol. 95, No. 3, July 1973, p. 342.

13 Tieu, A. K., "Oil-Film Temperature Distribution in an Infinitely Wide Slider Bearing: An Application of the Finite-Element Method," *Journal of Mechanical Engineering Science*, Vol. 15, No. 4, 1973, p. 311.

14 Huebner, K. H., "Application of Finite Element Methods to Thermohydrodynamic Lubrication," *International Journal of Numerical Methods in Engineering*, Vol. 8, No. 1, 1974, p. 139.

15 Shelly, P., and Ettles, C., "The Application of a Finite Element Method to the Evaluation of Oil Whirl Characteristics," *Journal of Mechanical Engineering Science*, I. Mech. E., Vol. 16, No. 2, 1974, pp. 101–108.

16 Huebner, K. H., *The Finite Element Method for Engineers*, Wiley, New York, 1975.

17 Waschpress, E. L., *Iterative Solution of Elliptic Systems and Applications to the Neutron Diffusion Equation of Reactor Physics*, Prentice-Hall, Englewood Cliffs. N. J., 1966.

18 Emery, A. F., and Carson, W. W., "Evaluation of the Use of the Finite Element Method in Computation of Temperature," *Journal of Heat Transfer*, TRANS. ASME, Series C, Vol. 93, No. 2, May 1971, pp. 136–145.

19 Hays, D. F., "Squeeze Films for Rectangular Plates," *Journal of Basic Engineering*, TRANS. ASME, June 1963, pp. 243–246.

APPENDIX

Equation (1) is solved using the fluidity matrix approach of [9]. The functional in equation (1) is broken up into integrals over the individual elements. Within each element, the pressure P is expressed in terms of the nodal pressures and linear interpolation functions [9]. The functional is then minimized by differentiating the total functional with respect to all unknown nodal pressures. This minimization produces the following set of matrix equations.

$$\begin{bmatrix} [K_p]_{11} & [K_p]_{12} & 0 & \cdot & 0 \\ [K_p]_{21} & [K_p]_{22} & [K_p]_{23} & \cdot & 0 \\ 0 & [K_p]_{32} & [K_p]_{33} & \cdot & 0 \\ \cdot & \cdot & \cdot & \cdot & \cdot \\ 0 & 0 & 0 & \cdot & [K_p]_{NN} \end{bmatrix} \times \begin{Bmatrix} \{P\}_1 \\ \{P\}_2 \\ \{P\}_3 \\ \cdot \\ \{P\}_N \end{Bmatrix} = - \begin{Bmatrix} \{K_{Ux}\}_1 \\ \{K_{Ux}\}_2 \\ \{K_{Ux}\}_3 \\ \cdot \\ \{K_{Ux}\}_N \end{Bmatrix} - \begin{Bmatrix} \{K_{Uy}\}_1 \\ \{K_{Uy}\}_2 \\ \{K_{Uy}\}_3 \\ \cdot \\ \{K_{Uy}\}_N \end{Bmatrix} - \begin{Bmatrix} \{K_{\dot{h}}\}_1 \\ \{K_{\dot{h}}\}_2 \\ \{K_{\dot{h}}\}_3 \\ \cdot \\ \{K_{\dot{h}}\}_N \end{Bmatrix} + \begin{Bmatrix} \{q\}_1 \\ \{q\}_2 \\ \{q\}_3 \\ \cdot \\ \{q\}_N \end{Bmatrix} \quad \text{(A.1)}$$

The Jth column of pressures is related only to the $J-1$th and $J+1$th column producing the tridiagonal form shown. The components of the pressure fluidity matrix $[K_p]$ are matrices of order $M \times M$ corresponding to the Jth column of M nodes. This may be written for the Jth column as

$$[K_p]_{J,J-1}\{P\}_{J-1} + [K_p]_{J,J}\{P\}_J + [K_p]_{J,J+1}\{P\}_{J+1} = -\{K_{Ux}\}_J - \{K_{Uy}\}_J - \{K_{\dot{h}}\}_J + \{q\}_J, \quad J = 1, 2, \ldots, N \quad \text{(A.2)}$$

where

$$[K_p]_{J,J} = \begin{bmatrix} K_{p11} & K_{p12} & 0 & \cdot & 0 \\ K_{p21} & K_{p22} & K_{p23} & \cdot & 0 \\ 0 & K_{p32} & K_{p33} & \cdot & 0 \\ \cdot & \cdot & \cdot & \cdot & \cdot \\ 0 & 0 & 0 & \cdot & K_{pMM} \end{bmatrix}_{J,J}$$

$$\{P\}_J = \begin{Bmatrix} P_1 \\ P_2 \\ P_3 \\ \cdot \\ P_M \end{Bmatrix}_J, \quad \{K_{Ux}\}_J = \begin{Bmatrix} K_{Ux1} \\ K_{Ux2} \\ K_{Ux3} \\ \cdot \\ K_{UxM} \end{Bmatrix}_J,$$

$$\{K_{Uy}\}_J = \begin{Bmatrix} K_{Uy1} \\ K_{Uy2} \\ K_{Uy3} \\ \cdot \\ K_{UyM} \end{Bmatrix}_J$$

$$\{K_{\dot{h}}\}_J = \begin{Bmatrix} K_{\dot{h}1} \\ K_{\dot{h}2} \\ K_{\dot{h}3} \\ \cdot \\ K_{\dot{h}M} \end{Bmatrix}_J, \quad \{q\}_J = \begin{Bmatrix} q_1 \\ q_2 \\ q_3 \\ \cdot \\ q_M \end{Bmatrix}_J$$

Only the subscripts outside the brackets change in writing similar expressions for $[K_p]_{J,J-1}$, $[K_p]_{J,J+1}$, and $\{P\}_{j-1}$, and $\{P\}_{J+1}$.

The individual components of all three types of block fluidity matrices are also tridiagonal in form. Considering first the lower diagonal block pressure fluidity matrix, the components associated with the I, Jth node are

$$K_{pI,I-1(J,J-1)} = K_{pjk}^{(I-1,J-1,1)} + K_{pkj}^{(I-1,J-1,2)} \tag{A.3}$$

$$K_{pI,I(J,J-1)} = K_{pki}^{(I-1,J-1,2)} + K_{pij}^{(I-1,J-1,4)} + K_{pik}^{(I,J-1,1)} + K_{pji}^{(I,J-1,3)} \tag{A.4}$$

$$K_{pI,I+1(J,J-1)} = K_{pjk}^{(I,J-1,3)} + K_{pkj}^{(I,J-1,4)} \tag{A.5}$$

The components of the main diagonal block pressure fluidity matrix are

$$K_{pI,I-1(J,J)} = K_{pji}^{(I-1,J-1,1)} + K_{pik}^{(I-1,J-1,4)} + K_{pij}^{(I-1,J,2)} + K_{pki}^{(I-1,J,3)} \tag{A.6}$$

$$K_{pI,I(J,J)} = K_{pjj}^{(I-1,J-1,1)} + K_{pkk}^{(I-1,J-1,2)} + K_{pii}^{(I-1,J-1,4)} + K_{pii}^{(I,J-1,1)} + K_{pjj}^{(I,J-1,3)} + K_{pkk}^{(I,J-1,4)} + K_{pii}^{(I-1,J,2)} + K_{pkk}^{(I-1,J,3)} + K_{pjj}^{(I-1,J,4)} + K_{pkk}^{(I,J,1)} + K_{pjj}^{(I,J,2)} + K_{pii}^{(I,J,3)} \tag{A.7}$$

$$K_{pI,I+1(J,J)} = K_{pij}^{(I,J-1,1)} + K_{pki}^{(I,J-1,4)} + K_{pji}^{(I,J,2)} + K_{pik}^{(I,J,3)} \tag{A.8}$$

Since

$$K_{pmn}^{(e)} = K_{pnm}^{(e)}$$

It is apparent that

$$K_{pI-1,I(J,J)} = K_{pI,I-1(J,J)} \tag{A.9}$$

so that the $[K_p]_{J,J}$ matrix is symmetric. The components of the upper diagonal block pressure fluidity matrix are

$$K_{pI,I-1(J,J+1)} = K_{pkj}^{(I-1,J,3)} + K_{pjk}^{(I-1,J,4)} \tag{A.10}$$

$$K_{pI,I(J,J+1)} = K_{pik}^{(I-1,J,2)} + K_{pji}^{(I-1,J,4)} + K_{pki}^{(I,J,1)} + K_{pij}^{(I,J,3)} \tag{A.11}$$

$$K_{pI,I+1(J,J+1)} = K_{pkj}^{(I,J,1)} + K_{pjk}^{(I,J,2)} \tag{A.12}$$

Comparing these components with equations (A.3)–(A.5) shows that

$$[K_p]_{J,J-1} = [K_p]_{J-1,J}^T \tag{A.13}$$

and the columns of the right-hand side of equation (A.2) are

$$K_{UxI(J)} = K_{Uxj}^{(I-1,J-1,1)} + K_{Uxk}^{(I-1,J-1,2)} + K_{Uxi}^{(I-1,J-1,4)} + K_{Uxi}^{(I,J-1,1)} + K_{Uxj}^{(I,J-1,3)} + K_{Uxk}^{(I,J-1,4)} + K_{Uxi}^{(I-1,J,2)} + K_{Uxk}^{(I-1,J,3)} + K_{Uxj}^{(I-1,J,4)} + K_{Uxk}^{(I,J,1)} + K_{Uxj}^{(I,J,2)} + K_{Uxi}^{(I,J,3)} \tag{A.14}$$

The expressions for the y shear and squeeze columns are the same as equation (A.14) except that Uy or $\dot{h}$, respectively, replaces Ux in the subscripts. Similarly, the boundary flow column is

$$q_{I(J)} = q_j^{(I-1,J-1,1)} + q_k^{(I-1,J-1,2)} + q_i^{(I-1,J-1,4)} + q_i^{(I,J-1,1)} + q_j^{(I,J-1,3)} + q_k^{(I,J-1,4)} + q_i^{(I-1,J,2)} + q_k^{(I-1,J,3)} + q_j^{(I-1,J,4)} + q_k^{(I,J,1)} + q_j^{(I,J,2)} + q_i^{(I,J,3)} \tag{A.15}$$

Certain subscript and superscript conventions apply to equations (A.3)–(A.15). On the left-hand side, the capital letter subscripts before the parentheses describe the position of the component within the block fluidity matrix or column and the capital letter subscripts inside the parentheses describe the position of the block fluidity matrix within equation (A.1). On the right-hand side, the first two capital letter superscripts give the nodal coordinates of the upper left-hand node associated with the element and the third superscript (a number) indicates the type of element. The small letter subscripts refer to the location of the element fluidity matrices and columns. Overall the capital letter subscripts range over the same values as the number of nodes

$$\left.\begin{array}{l} I = 1, 2, \ldots, M \\ \\ J = 1, 2, \ldots, N \end{array}\right\} \quad \text{subscripts}$$

while the capital letter superscripts in parentheses refer to the elements so they range over the values

$$\left.\begin{array}{l} I = 1, 2, \ldots, M-1 \\ \\ J = 1, 2, \ldots, N-1 \end{array}\right\} \quad \text{superscripts in parentheses}$$

It should be noted that these are completely general and that no problem requires that they all be calculated. First, the choice of 1–2 or 3–4 type elements is made which eliminates half of the terms. Second, since the main diagonal block pressure fluidity matrices are symmetric, equation (A.5) is not required. Equation (A.9) shows that the lower diagonal block pressure fluidity matrices are obtained from the transpose of the upper one or vice versa. Third, the boundary flow is evaluated only along the portion of the boundary where the flow is specified, C_q (usually not specified in lubrication problems) and all of the elements which do not have sides along C_q are not calculated. Of course all of these quantities are easily incorporated into an automatic computer program.

The elements are chosen small enough so that the parameters ρ, h, μ, U_x, U_y, $\partial h/\partial t$, and q_a are assumed constant within an element. The pressure, x shear, y shear, squeeze, and boundary flow fluidity matrices are

$$K_{pmn}^{(e)} = -\left[\frac{\rho h^3}{48\mu A}(b_m b_n + c_m c_n)\right]^{(e)} \tag{A.16}$$

$$K_{Uxn}^{(e)} = \left[\frac{1}{2}\rho h b_n U_x\right]^{(e)} \tag{A.17}$$

$$K_{Uyn}^{(e)} = \left[\frac{1}{2}\rho h c_n U_y\right]^{(e)} \tag{A.18}$$

$$K_{hn}^{(e)} = -\left[\frac{1}{3}\frac{\partial}{\partial t}(\rho h)A\right]^{(e)} \tag{A.19}$$

$$q_n^{(e)} = \left[\frac{1}{2}(q_x n_x + q_y n_y)C_q\right]^{(e)} \tag{A.20}$$

where the interpolation constants are

$$\begin{bmatrix} b_i & c_i \\ b_j & c_j \\ b_k & c_k \end{bmatrix}^{(e)} = \begin{bmatrix} y_j - y_k & x_k - x_j \\ y_k - y_i & x_i - x_k \\ y_i - y_j & x_j - x_i \end{bmatrix}^{(e)} \tag{A.21}$$

and the area is given by the determinant

$$2A^{(e)} = \begin{vmatrix} 1 & 1 & 1 \\ x_i & x_j & x_k \\ y_i & y_j & y_k \end{vmatrix} \tag{A.22}$$

Similar expressions may be found in [9].

The same analysis can be carried out for a rotating bearing such as a journal, partial arc, or multilobed bearing. Consider a shaft of radius R rotating with angular velocity ω_j in a journal bearing rotating with angular velocity ω_b. To maintain consistency in coordinate systems, unwrap the bearing and journal as in Fig. 5. Now, as before, the z-direction is across the film while an x and y may be used to locate the nodes. Equations (A.16), (A.19), and (A.20) remain the same while Equations (A.17) and (A.18) become

$$K^{(e)}_{Ixn} = \left[\frac{\rho h}{4} R(\omega_b + \omega_j) b_n\right]^{(e)} \tag{A.23}$$

$$K^{(e)}_{Iyn} = 0 \tag{A.24}$$

Note that $x = R\theta$ in equations (A.21) and (A.22).

DISCUSSION

S. M. Rohde[2]

The authors have presented some interesting numerical results pertaining to the application of finite element methods to lubrication problems. Their conclusions regarding mesh orientation and refinement agree with our own experience. In fact, in [20][3] an analysis of the linear equation at each node arising in both the finite difference and finite element formulations for the squeeze film problem was performed. Numerical comparisons similar to those presented in this paper were presented there. In particular, it was shown that the pressure distribution corresponding to (in the present paper) FEM #2 is everywhere greater than that of FEM #3.

A key and perhaps the most important point which the authors make is that for rectangular or "rectangular-like" regions the FEM topology becomes particularly simple leading to reduced bandwidth, etc. Furthermore, a large class of lubrication problems fall into this category. These facts were noted several years ago by the discussor [21]. Likewise it was also noted in [2] that such an "indexing" could be efficiently used to incorporate Reynold's boundary condition with an iterative scheme. More recently that construction was proven [22].

As noted in [21], any region which is "mappable" into a unit square can be indexed like the unit square. In this respect the unit square is a "canonical" region. Recent advances in automatic mesh generation [23, 24] have been based on precisely such mappings. We have recently used this approach (and some modifications) for generating two and three dimensional finite element discretizations. We will now illustrate the potential of the method of generating a FEM mesh via some examples. The reader is referred to [23, 24] for a complete treatment.

Basically, as shown in Fig. 7, a mapping is desired which maps the unit square S, $0 \le s \le 1$, $0 \le t \le 1$ onto the region R which is to be discretized. The mapping [25] is to take the interior of S onto the interior of R and the boundaries of S onto the boundaries of R. Every point in the interior of R is to be the image of a unique point in S. Denoting the four boundaries (curves) of R by $\mathbf{f}_i$ as shown, in Fig. 7 a bilinearly blended transfinite interpolant may be written as

$$\begin{Bmatrix} x(s,t) \\ y(s,t) \end{Bmatrix} = \mathbf{F}(s,t) = (1-s)\mathbf{f}_1(t) + s\mathbf{f}_2(t) + (1-t)\mathbf{f}_3(s) + t\mathbf{f}_4(s) - (1-s)t\mathbf{f}_1(1) - s(1-t)\mathbf{f}_2(0) - (1-s)(1-t)\mathbf{f}_3(0) - st\mathbf{f}_1(1)$$

Equation (1) provides a suitable mapping of the interior (and boundaries) of S onto the interior (and boundaries) of R. Our experience with equation (1), which represents the simplest form of the transfinite interpolant [23, 24], has been very good. To use this representation one merely programs the four parameterizations of the

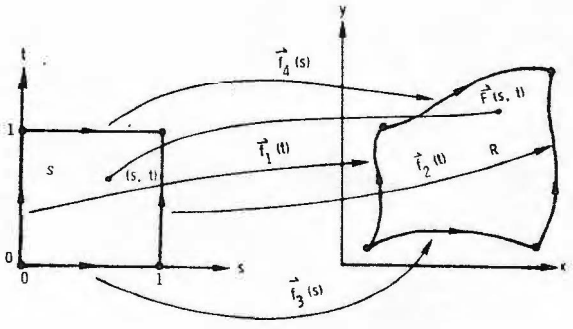

Fig. 7

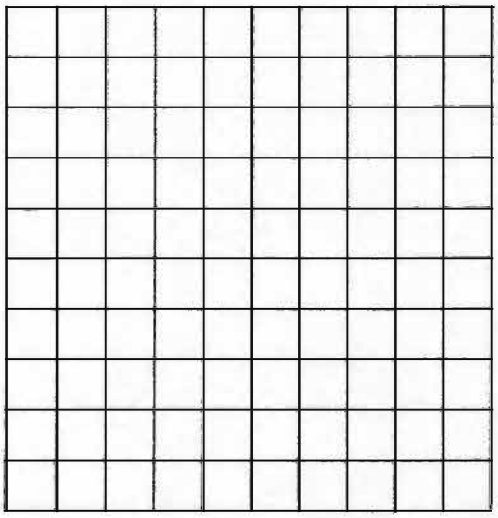

Fig. 8(*a*)

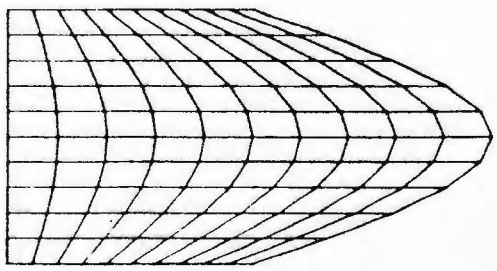

Fig. 8(*b*)

[2] Research Laboratories, General Motors Corp., Warren, Mich.

[3] Numbers in brackets designate Additional References at end of paper.

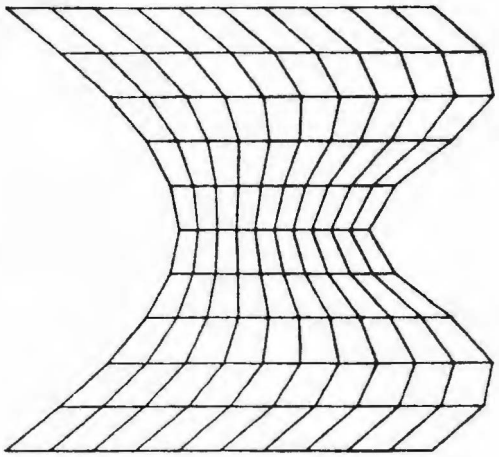

Fig. 8(c)

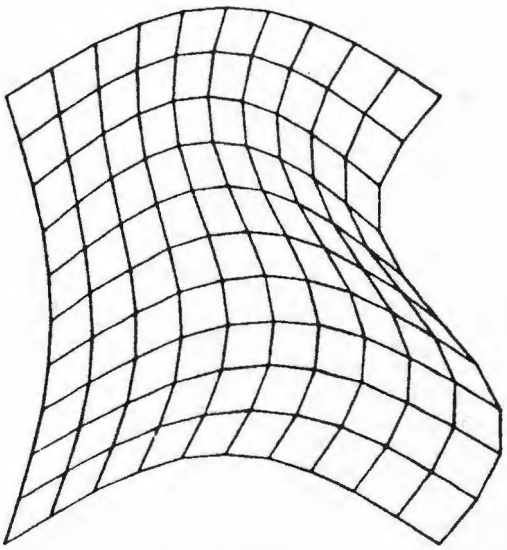

Fig. 8(d)

Fig. 8(e)

boundaries. Picking these parameterizations as well as the appropriate four boundaries can, however, sometimes require some experimentation. Here an interactive graphics terminal is almost mandatory. Figure 2a shows a uniform 10×10 mesh dividing S. Fig. 8(b) shows a simple mapping in which

$$\mathbf{f}_1(t) = \begin{Bmatrix} 0 \\ t \end{Bmatrix}$$

$$\mathbf{f}_2(t) = \begin{Bmatrix} 1 + \sin \pi t \\ t \end{Bmatrix}$$

$$\mathbf{f}_3(s) = \begin{Bmatrix} s \\ 0 \end{Bmatrix}$$

$$\mathbf{f}_4(s) = \begin{Bmatrix} s \\ 1 \end{Bmatrix}.$$

Fig. 8(c) shows a more severe situation in which

$$\mathbf{f}_1(t) = \begin{Bmatrix} 0.4 \sin \pi t \\ t \end{Bmatrix}$$

$$\mathbf{f}_2(t) = \begin{Bmatrix} 1 + 0.2 \sin 3\pi t \\ t \end{Bmatrix}$$

$$\mathbf{f}_3(s) = \begin{Bmatrix} s \\ 0 \end{Bmatrix}$$

$$\mathbf{f}_4(s) = \begin{Bmatrix} s \\ 1 \end{Bmatrix}.$$

In Fig. 8(d) we have

$$\mathbf{f}_1(t) = \begin{Bmatrix} 0.1 \sin \pi t \\ t \end{Bmatrix}$$

$$\mathbf{f}_2(t) \begin{Bmatrix} 1 + 0.15 \sin 2\pi t \\ t \end{Bmatrix}$$

$$\mathbf{f}_3(s) = \begin{Bmatrix} s \\ 0.2 \sin \pi s \end{Bmatrix}$$

$$\mathbf{f}_4(s) = \begin{Bmatrix} s \\ 1 + 0.2 \sin \pi s \end{Bmatrix}.$$

Finally in Fig. 8(e) we have

$$\mathbf{f}_1(t) = \begin{Bmatrix} 0.2(1 - t) \\ 0 \end{Bmatrix}$$

$$\mathbf{f}_2(t) = \begin{Bmatrix} 1 - 0.3((1 - t) \\ 0 \end{Bmatrix}$$

$$\mathbf{f}_3(s) = \begin{Bmatrix} 0.45 - 0.25 \cos \pi s \\ 0.25 \sin \pi s \end{Bmatrix}$$

$$\begin{Bmatrix} 0 \\ s \end{Bmatrix}, 0 \le S \le 0.3$$

$$\mathbf{f}_4(s) = \begin{Bmatrix} (s - 0.3)/0.4 \\ 0.3 \end{Bmatrix}, 0.3 < s \le 0.4$$

$$\begin{Bmatrix} 1.0 \\ (1.0 - s) \end{Bmatrix}, 0.7 < s \le 1$$

In conclusion it should be emphasized that the inclusion of an automatic mesh generation scheme such as presented in this discussion represents an extremely simple addition to a finite element lubrication code and is well worth the effort.

Additional References

20 Rohde, S. M., Discussion of "Application of Finite Element Methods to Lubrication: Squeeze Films between Porous Surface," by Eidelberg, B. E. and Booker, J. F., JOURNAL OF LUBRICATION TECHNOLOGY TRANS. ASME, Series F, Vol. 98, No. 1, Jan. 1976.

21 Rohde, S. M., "Finite Element Optimization of Finite Stepped Slider Bearing Profiles," *TRANS ASLE*. Vol. 17, 2, 1974.

22 Rohde, S. M. and McAllister, G. T., "A Variational Formulation for a Class of Free Boundary Problems Arising in Hydrodynamic Lubrication," *Int. J. Engrg. Sci.*, Vol. 13, 1975.

23 Gordon, William J., and Hall, Charles A., "Geometric Aspects of the Finite Element Method," in *The Mathematical Foundations of the Finite Element Method with Applications to Partial Differential Equations*, edited by A. K. Aziz, Academic Pres, New York, 1972.

24 Gordon, William J., and Hall, Charles A., "Construction of Curvilinear Co-ordinate Systems and Application to Mesh Generation," *Int. J. Num. Methods in Engineering*, Vol. 7, 1973, pp. 461-477.

J. F. Booker[4]

It is a good sign to find so many authors and discussors using the finite element method in lubrication. The method has come a long

[4] Associate Professor, School of Mechanical and Aerospace Engineering, Cornell University, Ithaca, N. Y.

way in quite a short time (as these things are measured).

The present paper and much of the earlier discussion centers on the mapping of bearing pads onto a generic rectangle for purposes of mesh generation. While this is certainly appropriate for many bearing and grooving geometries, the resulting regularity of nodal spacing is of some concern. One of the great putative advantages of the finite element method over the competing finite difference method is the ease with which meshes can be refined *locally* as required for solution accuracy. One hopes that this possibility is not being compromised too greatly in the schemes of the authors and discussors.

The authors have considered in some detail the matter of optimal mesh design. The finding that meshes should be finest in regions of high pressure gradients is, of course, not unexpected. It leads immediately to the awkward situation (found in other application fields as well) that the optimum *problem* formulation depends on the *solution*! The iterative process suggested by this paradox is being pursued actively in the structural mechanics field at present; perhaps some impact of that work will be felt in our own field before too long.

A. Curnier[5]

Along the plan followed by the authors, three subjects may be distinguished:

1 The pressure variational principle formulation which is quite classical and does not call for any comment;

2 the bandwidth minimization: the current trend is to relieve the user from being too much concerned with minimizing the bandwidth of his mesh by using, for instance, profile storage and solvers;

3 the mesh design optimizations: the paper provides very helpful practical guidelines for the user to design a near optimal mesh based on the intuitive picture of the solution:

(*a*) Align the diagonals dividing the preliminary quadrilaterals into the definitive triangular elements with the expected pressure gradient directions

(*b*) concentrate nodes where large pressure gradients are expected.

These two qualitative results can be explained and to some extent quantified as it is sketched now:

(*a*) Linear elements do preserve the continuity of pressure gradients inside an element and hereby along each side of the diagonal element interfaces: they do not preserve it across such diagonals. Result 3 (a) is a consequence of this remark..

(*b*) For a linear element used to solve a second order elliptic problem like the one at hand, the error pressure is expected to decrease as the square of the mesh refinement:

if p = exact pressure
p^h = f.e.m. pressure
h = mesh coarseness characteristic dimension (h = max $|h_j|$, h_j = side length of triangle j = 1,3
C = constant (element, p^h)
$||p||_s^2 = \int_\Omega (p^2 + p'^2 + \ldots + p^{(s)2}) d\Omega$
then $||p - p_h||_s = C_s h^{2-s}$ and in particular
$||p - p_h||_0 = C_0 h^2$

Therefore the only limitation on the rate of convergence (for a given problem and a given element) is the smoothness of the solution p.

The above rate of convergence is in the mean, for a regular mesh and without singularities. The pointwise convergence rate can be expected to be the same for a smooth solution and in fact

$$|p_e - p_{he}|_s \leq C_s h^{2-s} |p_e|_2$$

where e = element

$$|p|_s^2 = \int_\Omega (p^{(s)2}) d\Omega$$

Since h, μ, u_x, u_y are chosen constant over an element, the solution p exhibits singularities (probably more drastic as h decreases). With a regular mesh, the order of convergence will definitely be reduced. However, by properly grading the mesh (that is by keeping $h_e^{2-s} |p_e|_2$ roughly the same from one element to the next) the same order of accuracy can be achieved for a triangular as for a regular solution p.

Finally, it is recalled that the strict Ritz procedure always corresponds to an approximation which is too "stiff." The discrete energy exceeds the exact one which corresponds to an underestimate of the pressure gradients and pressures. This is true in the mean only since the link between energy and pressure is not strictly monotone. In other words p^h may exceed p in some parts of the mesh and still have smaller derivatives in the mean square sense. This can be changed by using a dual or hybrid formulation.

Results concerning rectangular and higher order elements can be obtained along the same lines.

[5] Ph.D. student, Division of Structural Engineering and Structural Mechanics, University of California, Berkeley, Calif.

Authors' Closure

The authors would like to thank the three discussers of the paper for their constructive comments. We are glad to see so much interest in the method developed here as we feel it provides detailed structure to material noted by other authors where little is explored in depth.

In the first discussion, substantial agreement with the authors work for the squeeze film problem is noted and some additional recent references are included. A useful mesh generation scheme particularly suited to the matrix labeling technique employed in the paper is presented. It appears to the authors that the matrix labeling facilitates automatic mesh generation of this and other types. In fact, the development of practical analysis computer programs for nonresearch engineers almost requires automatic schemes.

The second discusser is to be strongly commended for his excellent work in finite element analysis. It seems that the question of refining meshes locally has usually been done by adding a few extra nodes in the region where greatest accuracy is desired. Often in complex structural problems many of the nodes are assigned by hand so that adding another few nodes is much easier than regenerating a substantial portion of the mesh. Perhaps it is time to consider that the flexibility of the finite element method should be used to concentrate the grid points in the desired region using a combination of automatic mesh generation scheme and some sort of simple user assigned concentration factor. Simply adding a few nodes in one region can greatly increase the matrix bandwidth (and solution time) for the sake of only a few additional nodes. It should be emphasized again that the method developed in the paper does not depend in any way upon the regularity of nodal spacing but only on the regularity of the nodal numbering process. The relation between the two depends upon the ingenuity of the programmer.

In the third discussion the comments are more mathematical in nature. The continuity of pressure gradients preserved along the sides of elements, but not across them, has been observed by Oden [10] and other authors. Noting this point does, however, contribute to understanding the results for optimum alignment of the diagonals. Certainly much more work can be done with regard to other element configurations.

In the time since the paper was written and accepted for publication, the method described here has been applied to many practical applications. It has proved useful in analysing partial arc, axial groove. multilobe, tilting pad, and pressure dam bearings. In most industrial applications the load is known while the equilibrium position must be found by an iterative process. A coarse grid system using approximately 3 axial node points and 9 circumferential node points per pad is used to obtain a first estimate of the equilibrium eccentricity

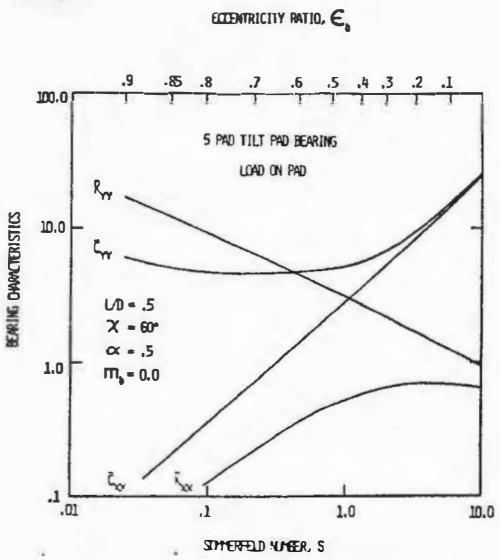

Fig. 9 Bearing characteristics versus Sommerfeld number and eccentricity ratio for a 5 pad tilt pad bearing

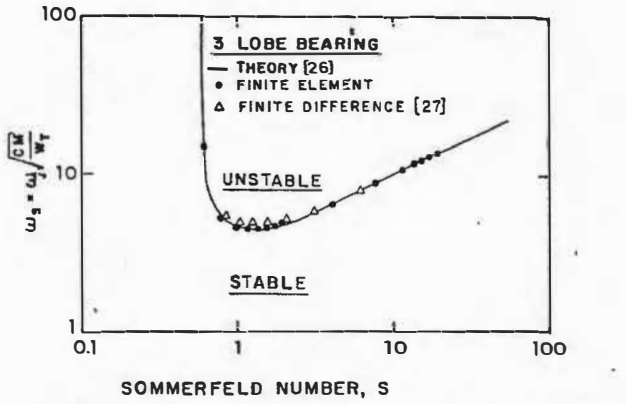

Fig. 10 Stability threshold versus Sommerfeld number for three pad multilobe bearing. 100° pad arc length, offset factor 0.8, preload 0.7, load on center of pad, $L/D = 0.75$

and attitude angle. Then a full grid system of, say, 5 by 31 nodes per pad is employed. For eccentricities around 0.5, this reduces the number of full grid iterations to 2 or 3. A casual survey of computer execution times indicates approximately a 50 percent saving by using the coarse grid system. Numerical differentiation is then used to determine dynamic coefficients and the Routh criteria used for the stability of each bearing. Thus even the linearized bearing analysis, as opposed to a transient one, for a four pad multilobe bearing can involve 36 solutions of Reynolds equation to obtain the equilibrium position. This includes taking four pads per evaluation, three evaluations to determine the appropriate slopes for a Newton Raphson iterative process, and three iterations. Furthermore, 32 more evaluations are required to determine the dynamic coefficients (taking four pads and central differences for the coefficients). The situation is much worse for tilt pad bearings when pad iterations are necessary. Clearly the consideration of error and computer time saving is not merely academic.

To further demonstrate the practical applicability of the method outlined in this paper, Fig. 9 presents stiffness and damping coefficients for a 5 pad tilt pad bearing. These coefficients were determined using the finite element analysis outlined here and the pad assembly method [25].[6] These coefficients may be used in critical speed and stability programs when rotor-bearing systems are analyzed. Also, these coefficients may be employed in a linear time transient program. Finally, the characteristics may be used in a simple stability analysis for the bearing. A sample stability curve is shown in Fig. 10 for a 3 pad multilobe bearing where

$$L/D = .75$$

$$\chi = 100°$$

$$\alpha = .8$$

$$m_b = .7$$

and the loading is on the center of the bottom pad. The finite element solution is compared to a long bearing solution with end leakage correction [26] and a finite difference solution [27]. The stability parameter, ω_s, is discussed in detail in references [26] and [28].

Additional Nomenclature

c = pad radial clearance, (mm)

c_b = bearing radial clearance, (mm)

C_{xx}, C_{yy} = principal horizontal, vertical damping coefficients, (N-s/mm)

$\bar{C}_{xx}$, $\bar{C}_{yy} = C_{xx}\frac{c\omega_j}{W_T}$, $C_{yy}\frac{c\omega_j}{W_T}$, dimensionless principal horizontal, vertical damping coefficients

D = bearing diameter, (mm)

K_{xx}, K_{yy} = principal horizontal, vertical stiffness coefficients, (N/mm)

$\bar{K}_{xx}$, $\bar{K}_{yy} = K_{xx}\frac{c}{W_T}$, $K_{yy}\frac{c}{W_T}$, dimensionless principal horizontal, vertical stiffness coefficients

L = bearing length (mm)

M' = journal mass (N-s^2/mm)

$m_b = 1 - \frac{c_b}{c}$, bearing preload factor

N_j = journal rotational speed, (rev/s)

$S = \frac{\mu N_j LD}{W_T}\left(\frac{R}{c}\right)^2$, Sommerfeld number

W_T = bearing external load, (N)

$\alpha = \frac{\theta_p}{\chi}$, bearing offset factor

ϵ_b = bearing eccentricity ratio

θ_p = angle from leading edge of pad to pad pivot point, (degrees)

χ = pad arc length, (degrees)

$\omega_s = \omega_j \sqrt{\frac{cM'}{W_T}}$, stability parameter

[6] Numbers 25–28 in brackets designate Additional References at end of closure.

Additional References

25 Lund, J. W., "Spring and Damping Coefficients for the Tilting-Pad Journal Bearing," *Trans. ASLE*, Vol. 7, No. 4, Oct. 1964, pp. 342–352.

26 Eierman, R. M., "Stability Analysis and Transient Motion of Axial Groove, Multilobe, and Tilting Pad Bearings," MS thesis, University of Virginia, Aug. 1976.

27 Lund, J. W., "Rotor-Bearing Dynamics Design Technology, Part VII: The Three Lobe Bearing and Floating Ring Bearing," Mechanical Technology Incorporated, Technical Report No. AFAPL-TR-65-45, Feb. 1968.

28 Barrett, L. E., Gunter, E. J., and Allaire, P. E., "Stability and Dynamic Response of Pressurized Journal Bearings with Nuclear Water Pump Applications," to be published in *Annals of Nuclear Energy*.